Bacterial predation on T4 phages

Jean-Jacques Godon[a], Ariane Bize[b], Hoang Ngo[b], Laurent Cauquil[c], Mathieu Almeida[d], Marie Agnès Petit[e], Olivier Zemb[c].

Affiliations

[a]INRAE, Univ Montpellier, LBE, Narbonne, France, 11100

[b]INRAE, Hydrosyst & Bioproc Res Unit, Antony, France, 92160

[c]INRAE, Univ Toulouse, ENVT, GenPhySE, Toulouse, France, 31320

[d]INRAE, MetaGenoPolis, Jouy-en-Josas, France, 78350

[e]Université Paris- Saclay, INRAE, AgroParisTech, Micalis Institute, Jouy-en-Josas, France, 78350

* Paste corresponding author name(s) here.

Email: olivier.zemb@inrae.fr

Author Contributions: J.J.G., O.Z., A.B. and N.H. designed and performed the experiments; J.J.G., O.Z., L.C. and M.A. performed computational experiments; J.J.G., O.Z., L.C., M.A. and M.A.P. contributed lineaging data and expertise; J.J.G. and O.Z.

prepared the manuscript with assistance from all authors; J.J.G. and O.Z. supervised and directed the research.

Competing Interest Statement: no competing interest.

Classification: Microbiology

Keywords: bacteriophage, Aeromonas, Stable-isotope probing

Abstract

Background: Bacterial consumption of viruses has never yet been reported, even though bacteria feed on almost anything. Viruses are omnipresent predators for all organisms, but have no acknowledged active biocontrol. The viral biomass undoubtedly reintegrates the trophic cycles, however the mechanisms of this phase still remain unknown.

Methods: Here, we used stable isotope probing with ^{13}C labelled T4 phages to monitor the increase of density of the bacterial DNA concomitant with the decrease of plaque forming units. We used ^{12}C T4 phages as control.

Results: T4 phage disappearance in wastewater sludge was found to occur mainly through predation by *Aeromonadacea*. Phage consumption also favours significant *in situ* bacterial growth. Furthermore, an isolated strain of *Aeromonas* was observed to grow on T4 phages as sole source of carbon, nitrogen and phosphorus.

Conclusions: bacterial species are capable of consuming bacteriophages *in situ*, which is likely a widespread and underestimated type of biocontrol. This assay is anticipated as a starting point for harnessing the bacterial

potential in limiting the diffusion of harmful viruses within environments such as gut or water.

Introduction

For any type of bacteria, the presence of viruses may present a significant opportunity for feeding. Indeed, viruses represent 0.2 gigatons of carbon on Earth(Bar-On *et al.*, 2018). For example, the major capsid protein of the T4-like bacteriophage family is one of the most prevalent proteins in the biosphere(Comeau and Krisch, 2008). Therefore phages represent a major potential carbon source into which bacteria may tap. Furthermore, viruses are also a potential source of phosphorus(Jover *et al.*, 2014).

No bacterium preying on viruses have been described even though bacterial extracellular proteases are able to degrade certain bacteriophages in anaerobic wastewater treatment plants, in pure cultures(Mondal *et al.*, 2015) and in soil(Nasser *et al.*, 2002). In seawater, the only reported biotic pressure arises from marine ciliates that have been co-incubated with viruses and bacteria(Gonzalez and Suttle, 1993). This observation is also supported by the recent discovery of viral DNA in free-living eukaryotic cells(Brown *et al.*, 2020).

Here, we show that specific bacteria can indeed degrade T4 bacteriophages *in situ*, and we confirm this observation in pure culture.

Results

When searching for bacteriophage consumption activity, sludge from wastewater treatment plants is a relevant microbiota to investigate, as it boasts a high degradation capacity. In this work, the stable isotope probing method was applied by adding 2.2 10^{10} ^{13}C-labelled T4 phages to 200 µl of sludge corresponding to 10^{8} bacteria cells. The increase in density of the bacterial DNA of the ^{12}C control bottle was then measured after the enumerated T4 phages decreased by 99%.

T4 phages were assimilated by bacteria. About 41% of the ^{13}C atoms initially present in T4 phages were accounted for in the bacterial biomass. However, only nine out of the 4046 microbial species - or more accurately Amplicon Sequence Variant (ASVs) - were labelled by the ^{13}C initially contained in the T4 phages (Fig. 1), thus suggesting that the incorporation of T4 phage is not a widespread ability. This incorporation generated growth, since the total biomass increased 2 fold after 24h concomitantly with the disappearance of the T4 phages.

The two main degraders of T4 phages were ASV1 (*Aeromonas sp.)* and ASV2 (*Tolumonas* sp.), which accounted for 5% and 29% of ^{13}C atoms found in the bacterial biomass respectively. Both belong to the *Aeromonadaceae* family and exhibit strong growth rates. Indeed, both rose from undetectable levels to 51% of the biomass, while the density of their DNA increased because they incorporated ^{13}C atoms from the isotopically

labelled T4 phages. For example, the 2 10^6 *Aeromonas* cells present after 24h contained 85% of ^{13}C atoms in their DNA whose density shifted from 1.72 g/mL to 1.75 g/mL in the bottle with ^{13}C-labeled T4 phages. The 16S rRNA sequences assigned to *Aeromonas* represented 19% and 8% of the total reads in the ^{12}C and the^{13}C bottles respectively, thus revealing a consistent growth from initially undetectable levels.

In addition to the *Aeromonadaceae* family, two species (ASV12 and 21) belonging to the Ignavibacteriales PHOS-HE36 family, although labelled with medium strength (49 and 71%) and negligible growth (0 and 5.87 10^6 synthetized cells respectively), still gathered 5% of the ^{13}C atoms. The last 5 species with significant DNA density shifts (ASV7, 9, 20, 67 and 79) accounted for the remaining 1% of ^{13}C atoms but their weak labelling level may have resulted from indirect labelling.

To confirm the quality of *Aeromonas sp.* as a predator of T4 phages, an *Aeromonas*-selective medium was used for retrieving an *Aeromonas* colony from the initial sludge and called it Aeromonas_isolate_007. The analysis of the whole genome confirmed that this isolate belongs to an intermediate clade between *Aeromonas media* and *Aeromonas rivipollensis* species. Aeromonas_isolate_007 was incubated with T4 phages as only substrate. Starting with 50 resting bacterial cells, the population reached 1.6 10^8 cells after 24 hours at 20°C while consuming 10^{11} T4 phages (Fig. 1C). No growth was observed when T4 phages were absent.

Aeromonas sp. can also capture T4 phages when their concentrations were comparable with environmental conditions: $7\,10^4$ T4 phages/mL decreased to $2\,10^3$ T4 phages/mL when incubated with Aeromonas_isolate_007 cells (Fig 1C). No decrease in the T7 phage has been observed in similar experiments where the T4 phage was replaced by the T7 phage.

Discussion

Aeromonas cells are present in virtually any environment(Janda and Abbott, 2010), including wastewater treatment plants where their abundance is around 0.1 %(Ye *et al.*, 2012).

Interestingly, *Aeromonas* cells have an S-layer(Noonan and Trust, 1997) associated with lipopolysaccharides (Sleytr *et al.*, 2014) and an outer membrane protein C, which are known to bind the T4 phages to the surface of *E.coli* cells(Islam *et al.*, 2019). Once captured at the surface, the phage is likely degraded by several extracellular enzymes, including DNase and protease (Janda, 1985). For example, metallo- and serine- proteases found in *Aeromonas* are involved in the degradation of large molecules such as albumin, earning the nickname of 'Jack-of-all-trades' due to this enzymatic versatility(Seshadri *et al.*, 2006). Finally, *Aeromonas* possesses transporters to uptake the resulting amino acids and peptides (Seshadri *et al.*, 2006).

Bacterial predation on bacteriophages is rich in consequences because bacteriophages are ultimate predators at the top of all food chains since they are not hunted. Indeed bacteriophage decay is mainly considered abiotic via adhesion to particulate material, chemical inactivation or degradation by solar radiation or passive grazing by flagellates(González and Suttle, 1993). In the oceans, this predation likely allows for the upper levels of the trophic chain carbon to access to the 7% of dissolved nitrogen, the 5% of phosphorus and the 1% of dissolved organic carbon contained in the viral particles (Jover *et al.*, 2014).

Furthermore, the diversity in bacteriophages could be partly related to the presence of phage-specific bacterial bacteriophage-hunters. Indeed, the bacterial predators of T4 phages do not appear to consume T7 bacteriophages. Therefore, brutal increase of a specific phage in the environment could be specifically controlled by a phage-eating bacterium, forming a killing-the-killer loop.

In conclusion, bacteria that are capable of eliminating specific viruses changes our vision of the food webs and represent a noteworthy avenue to explore to control harmful viruses such COVID-19, bacteriophages that disrupt dairy fermentations or rotaviruses causing diarrhoea.

Declarations

131 Ethics approval and consent to participate

132 Not Applicable

133 Consent for publication

134 Not Applicable

135 Availability of data and materials

136 High-throughput sequencing data have been deposited on NCBI
137 (https://www.ncbi.nlm.nih.gov/bioproject) under accession number PRJNA650397
138 and the genome of Aeromonas_isolate_007 is accessible with the BioSample
139 accession number SAMN17689348.

140 Competing Interests statement

141 The authors declare that they have no competing interests.

142 Funding

143 The work was funded by the French National Research Institute for Agriculture, Food
144 and Environment (INRAE).

145 Contributions

J.J.G., O.Z., A.B. and N.H. designed and performed the experiments; J.J.G., O.Z., L.C. and M.A. performed computational experiments; J.J.G., O.Z., L.C., M.A. and M.A.P. contributed lineaging data and expertise; J.J.G. and O.Z. prepared the manuscript with assistance from all authors; J.J.G. and O.Z. supervised and directed the research.

Acknowledgments

We thank Caroline Achard for insights on bacteriophage capture, Martin Beaumont and Amira Bousleh for the qPCR of the internal standard. Electronic microscopy work has benefited from the facilities and expertise of MIMA2 MET – GABI, INRA, Agroparistech, 78352 Jouy-en-Josas, France. Sequencing was performed in collaboration with the GeT core facility, Toulouse, France (http://get.genotoul.fr) supported by France Génomique National infrastructure, funded as part of “Investissement d’avenir” program managed by the Agence Nationale pour la Recherche (contract ANR-10-INBS-09). Figure 1 was created by Biorender.

Authors' information

JJG directed the PhD of OZ in bacterial ecology in France. In a following postdoc, OZ learned stable-isotope probing in sludge in Australia and was granted a small project to study the adsorption of T2 phages in the light of electrostatics. The combination of SIP and phage expertise turned out useful to answer JJG’s question about the predation of phages together with AB, which has expertise in producing purified isotopically-labeled

phages and MAP, which could confirm the results in pure culture with JJG since an isolate was successfully isolated from the sample. MA's expertise in genome annotation was put to use to speculate about the mechanisms involved in the capture, digestion and assimilation of T4 phages by bacteria.

References

Bar-On YM, Phillips R, Milo R (2018). The biomass distribution on Earth. *Proceedings of the National Academy of Sciences* **115:** 6506-6511.

Brown JM, Labonté JM, Brown J, Record NR, Poulton NJ, Sieracki ME *et al* (2020). Single Cell Genomics Reveals Viruses Consumed by Marine Protists. *Front Microbiol* **11:** 524828.

Comeau AM, Krisch HM (2008). The capsid of the T4 phage superfamily: the evolution, diversity, and structure of some of the most prevalent proteins in the biosphere. *Mol Biol Evol* **25:** 1321-32.

Gonzalez JM, Suttle CA (1993). Grazing by Marine Nanoflagellates on Viruses and Virus-Sized Particles - Ingestion and Digestion. *Marine Ecology-Progress Series* **94:** 1-10.

González JM, Suttle CA (1993). Grazing by marine nanoflagellates on viruses and virus-sized particles: ingestion and digestion. *Marine Ecology Progress Series* **94:** 1-10.

Islam MZ, Fokine A, Mahalingam M, Zhang Z, Garcia-Doval C, van Raaij MJ *et al* (2019). Molecular anatomy of the receptor binding module of a bacteriophage long tail fiber. *PLOS Pathogens* **15:** e1008193.

Janda JM (1985). Biochemical and exoenzymatic properties of Aeromonas species. *Diagnostic Microbiology and Infectious Disease* **3:** 223-232.

188 Janda JM, Abbott SL (2010). The genus Aeromonas: taxonomy, pathogenicity, and infection. *Clin*
189 *Microbiol Rev* **23:** 35-73.

190 Jover LF, Effler TC, Buchan A, Wilhelm SW, Weitz JS (2014). The elemental composition of virus
191 particles: implications for marine biogeochemical cycles. *Nat Rev Microbiol* **12:** 519-28.

192 Mondal T, Rouch DA, Thurbon N, Smith SR, Deighton MA (2015). Factors affecting decay of
193 Salmonella Birkenhead and coliphage MS2 during mesophilic anaerobic digestion and air drying
194 of sewage sludge. *J Water Health* **13:** 459-72.

195 Nasser AM, Glozman R, Nitzan Y (2002). Contribution of microbial activity to virus reduction in
196 saturated soil. *Water Res* **36:** 2589-95.

197 Noonan B, Trust TJ (1997). The synthesis, secretion and role in virulence of the paracrystalline
198 surface protein layers of Aeromonas salmonicida and A. hydrophila. *FEMS Microbiol Lett* **154:** 1-
199 7.

200 Seshadri R, Joseph SW, Chopra AK, Sha J, Shaw J, Graf J *et al* (2006). Genome Sequence of
201 Aeromonas hydrophila ATCC 7966^T: Jack of All Trades. *Journal of*
202 *Bacteriology* **188:** 8272-8282.

203 Sleytr UB, Schuster B, Egelseer E-M, Pum D (2014). S-layers: principles and applications. *FEMS*
204 *Microbiology Reviews* **38:** 823-864.

205 Ye L, Zhang T, Wang T, Fang Z (2012). Microbial structures, functions, and metabolic pathways in
206 wastewater treatment bioreactors revealed using high-throughput sequencing. *Environ Sci*
207 *Technol* **46:** 13244-52.

208

209

210

211

212

Figure 1. Bacterial growth on T4 phages. **A; Identification of ^{13}C-labeled bacteria:** the ^{13}C-labeled T4 (red) were incubated with a microbial community of wastewater treatment plant in the same conditions as the ^{12}C control (blue). **B; Bacteria present in each sample:** the barplots shows the growth of each ASVs based on 16S rDNA copies, detailing the nine bacteria assimilating T4 phages. **C; The density plots show the shift in density for ASV1 (*Aeromonas* sp.)**, which was abundant in both bottles after 24h. **D; ^{13}C labelling level after 24h:** the ^{13}C-labeling level (left Y-axis), computed from the individual density shifts (right Y-axis), is reported against the initial abundance of the ASVs (X-axis). The volume of the spheres represents the abundance of each ASV in the ^{13}C bottle. **E; *Aeromonas* sp. growth on T4 phages:** Aeromonas_isolate_007 grew on T4 phages as sole carbon and nitrogen source. When a few *Aeromonas* cells were incubated with 10^{11} T4 phages, the colony forming units (brown) increased while the plaque-forming units (blue) decreased.

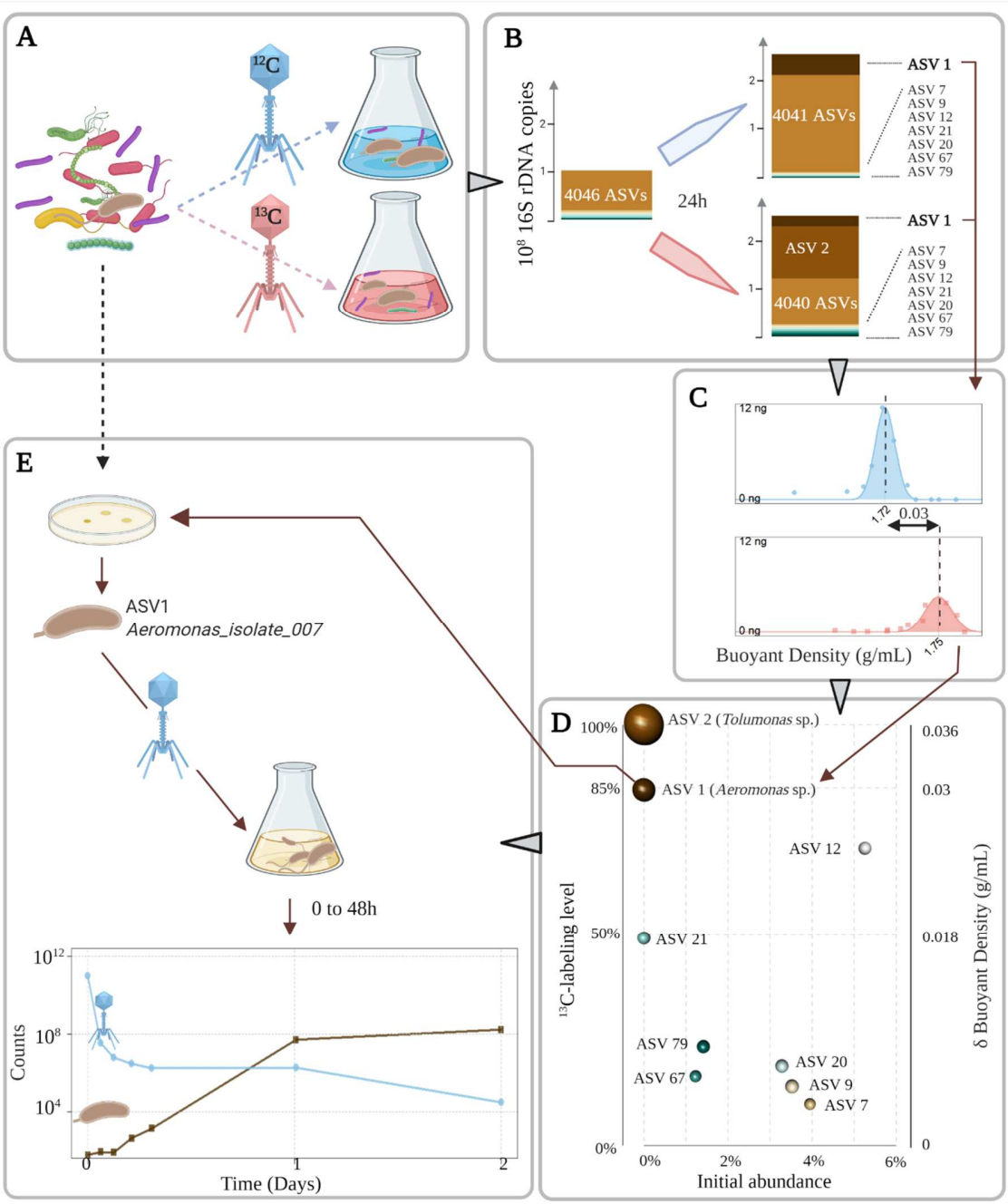
A
12C
13C
B
10⁸ 16S rDNA copies
4046 ASVs
24h
4041 ASVs
4040 ASVs
ASV 2
ASV 1
ASV 7
ASV 9
ASV 12
ASV 21
ASV 20
ASV 67
ASV 79
C
12 ng
0 ng
1.72
0.03
1.75
Buoyant Density (g/mL)
D
100%
85%
50%
0%
ASV 2 (Tolumonas sp.)
ASV 1 (Aeromonas sp.)
ASV 12
ASV 21
ASV 79
ASV 67
ASV 20
ASV 9
ASV 7
13C-labeling level
δ Buoyant Density (g/mL)
0.036
0.03
0.018
0
0%
2%
4%
6%
Initial abundance
E
ASV1
Aeromonas_isolate_007
0 to 48h
Counts
Time (Days)

228

Supplementary information

TABLE OF CONTENT

LIST OF FIGURES

LIST OF TABLES

1 Stable isotope probing experiment on the initial sample

1.1 Preparation of the ^{13}C-labeled T4 bacteriophages

T4-phage particles labeled with ^{13}C were produced on *Escherichia coli* B cells (DSM 613) grown in M9 minimal medium with ^{13}C-glucose as the sole carbon source. The M9 medium was prepared using M9, Minimal Salts, 5X (Sigma-Aldrich), by adding MgSO4 (Sigma-Aldrich) and CaCl2 (Sigma-Aldrich) at final concentrations of 1 mM, and D-Glucose at a final concentration of 10 g/L. Moreover, additional salts were added to favor phage adsorption (solution of CaCl2 0.5 M and MgCl2 1M, diluted 1 000 times in the culture medium). More precisely, starting from an *E. coli* stock of cells frozen in LB and glycerol, two successive overnight pre-cultures were grown in LB medium (LB broth, Fisher). Subsequently, 5 x 20 mL of M9 minimal medium containing D-Glucose-^{13}C6 as the sole carbon source (10 g/L) were each inoculated with 20 µL of the second *E. coli* pre-culture; approximately 1500 T4-phage particles (DSM 4505, in PFU) were added. Finally, 20 µL of a solution containing 0.5 M CaCl2 and 1M MgCl2 were also added in each case to favor phage adsorption.

After 30 hours of incubation at 37°C under agitation, the T4 phage particles were collected: the cultures were centrifuged during 15 minutes at 5 000 g, 10°C. The supernatants were collected and filtered at a 0.22 µm pore-size (PES filters, Milipore). They were subsequently incubated overnight in 8% w/v PEG 6000 and 0.5 M NaCl solution, at 4°C, to precipitate viral particles. The supernatants were centrifuged at 20 000g, during 30 minutes, at 4°C. The pellets were suspended in SM buffer (100 mM NaCl, 8 mM MgSO4, 50 mM Tris pH 7.5), and centrifuged once more at 20 000 g for 4h at 4°C. Viral particles were finally suspended in 1.4 mL of SM buffer and stored at 4°C before use.

To obtain unlabeled T4 phage particles, the same procedure was used except that unlabeled glucose was employed in the M9 minimal medium.

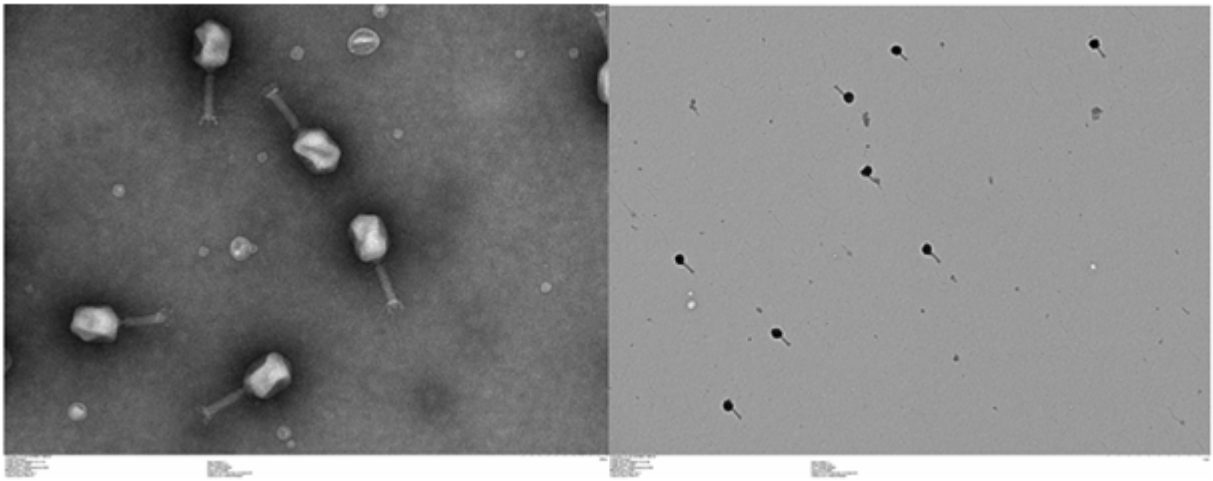

Figure S 1 : Purity of the bacteriophage preparation

We checked the purity of the bacteriophage preparation by electronic microscopy. Materials were directly adsorbed onto a carbon film membrane on a 300-mesh copper grid, stained with 1% uranyl acetate, dissolved in distilled water, and dried at room temperature. Grids were examined with Hitachi HT7700 electron microscope operated at 80kV (Elexience – France), and images were acquired with a charge-coupled device camera (AMT).

Table S 1 : Decrease of the free ^{13}C and ^{12}C bacteriophages by PFU of the supernatant. We indicate the absolute numbers of phages and their percentages compared to t_0.

Time (min)	T4 phages in ^{12}C bottle	T4 phages in ^{13}C bottle	T4 phages in ^{12}C bottle	T4 phages in ^{13}C bottle
0	$2.8\ 10^{10}$	$2.2\ 10^{10}$	100 %	100 %
24	$5.2\ 10^{8}$	$9.4\ 10^{8}$	1.9 %	4.2 %
122	$2.6\ 10^{7}$	$4.1\ 10^{8}$	0.9 %	1.8 %
445	$3.2\ 10^{7}$	$3.3\ 10^{8}$	1.2 %	1.5 %
1375	$5\ 10^{2}$	$5.7\ 10^{5}$	0 %	0 %

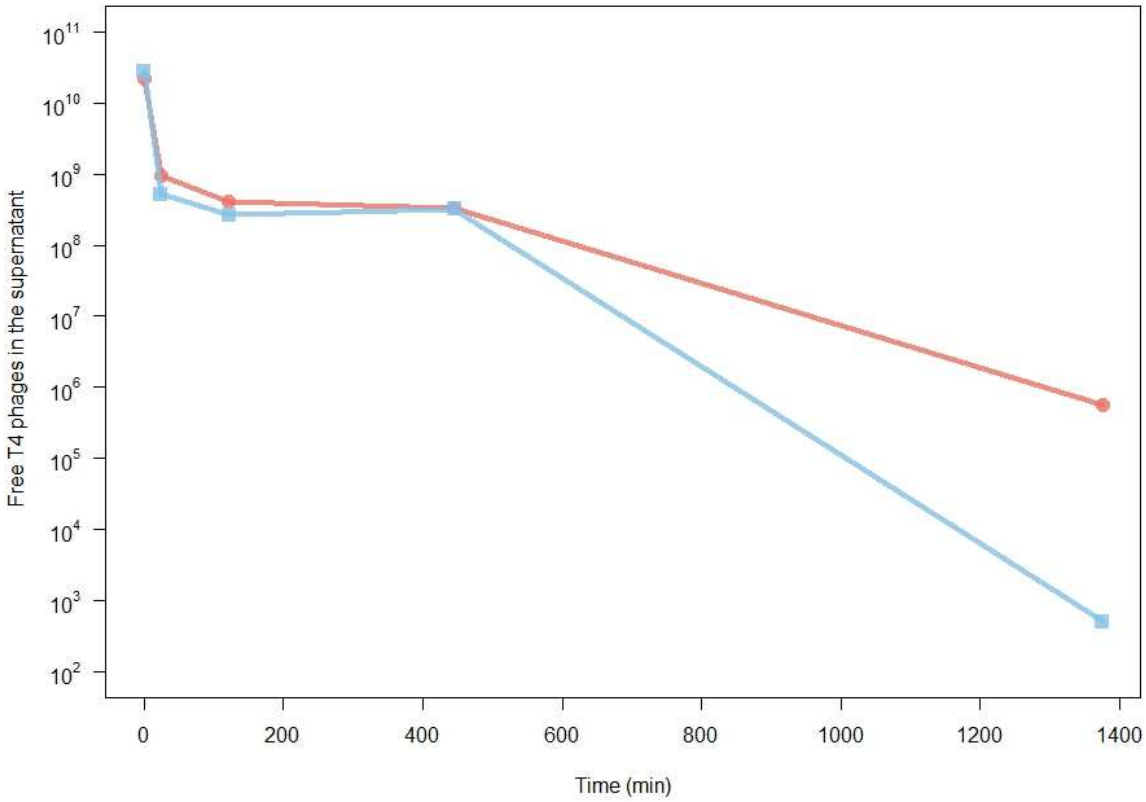

Figure S 2: Decrease of the free ^{13}C and ^{12}C bacteriophages by PFU of the supernatant

Free purified T4 phages were incubated with the initial sample of wastewater treatment plant. The initial concentration was $2.24\ 10^{10}$ T4 phages in 5 mL, i.e. $4.48\ 10^{9}$ T4 phages/mL. After 24h, over 99% of the T4 phages are missing from the supernatant due to incorporation or absorption into the microbial biomass. The red curve represents the ^{13}C bottle and the blue curve represents the ^{12}C bottle. The PFU titers of the obtained 13C- and unlabeled T4 stock solutions were determined on a bacterial lawn of E. coli cells (DSM 613), using the soft-agar overlay technique. More precisely, 5 µL of T4 phage stock solutions and serial dilutions of them (factor 10 or 15) were plated a soft layer containing 7.5 g/L of Agar and E.coli cells (DSM 613) pre-cultured in LB medium, in LB-Agar plates (15 g/L of Agar, Sigma-Aldrich). After a short period of drying, the Petri dishes were incubated at 37°C during 24 hours in static conditions. The PFU titers were determined by counting the visible plaques and calculating the concentration in the original stock solutions.

1.2 Detailed Calculations of the ^{13}C mass balance

This paragraph explains in details the calculations reported in Table S3. For a simpler explanation, we will focus here on the calculations about ASV1 (*Aeromonas* sp.).

STEP1: using qPCR, we determine the absolute abundance of bacteria in the ^{13}C bottle at the beginning of the experiment and at the end of the experiment. This can be done because we spiked 3 10^5 copies of a synthetic DNA standard to 200 µl of the initial sample [1], which we extracted immediately and quantified using 16S universal primers. We also spiked the final pellet with 3 10^5 copies of a synthetic DNA standard and quantified it using specific primers. The comparison of the 16S and internal standard qPCR curves indicates that the initial sample contained $1.798^{23.462}/1.828^{13.215}$=326 fold more bacterial 16S rDNA copies than internal standard (Table S 2), so that the tube contained 3 10^5 x 326 = 9.78 10^7 copies of bacterial 16S at the beginning of the experiment. At the end of the experiment, comparing the 16S and internal standard qPCR curves indicates that bacterial 16S rDNA were 783 fold more abundant than the spiked synthetic standard, leading to an estimated 2.35 10^8 copies of bacterial 16S rDNA genes in the ^{13}C bottle. For an accurate mass balance, we also consider the fact that 240 µl were taken out for PFU measurements during the experiment, so that we estimate that 2.47 10^8 copies of 16S rDNA would have been present at the end of the experiment in the ^{13}C bottle if no sampling had been performed. Since we used the LinReg software, we also accounted for the slight individual variations in qPCR efficiency, which were between 80 and 84% for the internal standard and between 80 and 82% for the bacterial 16S rRNA genes respectively. In total, we estimate a global biomass increase of 2.35 fold. This global increases regroups ASVs that are initially abundant and grow slightly with ASVs that are initially rare and grow massively.

Table S 2 : Quantification of the bacterial density with the internal standard at the beginning and at the end of the experiment.

Sample name	Primers	Efficiency	Cycle Threshold	Spiked internal standard	16S rDNA
Initial_sample	Internal standard	79.8 %	23.462	3 10^5 copies	9.78 10^7 copies
	V4V5	82.8%	13.215		
Final_^{13}C_sample	Internal standard	80.1%	14.133	3 10^5 copies	2.35 10^8 copies
	V4V5	84.5%	24.461		

STEP2: using 16S metabarcoding, we use the absolute abundance of 16S rDNA of each ASV at the beginning and at the end of the experiment to estimate the number of 16S rDNA copies produced during the experiment for each ASV. ASV1 (*Aeromonas* sp.) was undetectable in the 3748 sequences of 16S rRNA genes obtained at the beginning of the experiment. At the end, 303 sequences out of 3578 (i.e. 8%) belonged ASV1 (*Aeromonas* sp.). For the two instances where the final 16SrDNA abundances were lower than the initial 16S rDNA abundances (possibly due to part of the population dying combined with another part showing a small growth), we neglected the contribution of these ASVs to the ^{13}C mass balance.

STEP3: using a database of 16S rDNA copy number[2], we convert the increase in 16S rDNA into the number of cells. *Aeromonas* has 10 copies of 16S rDNA, so that 2.09 10^7 copies of 16S rDNA corresponds to 2.09 10^6 *Aeromonas* cells. ASV 1 was undetectable at t_0, so that if only one cell of ASV 1 (*Aeromonas* sp.) was present at the beginning of the experiment, 22 generations would have

been needed in the course of the experiment to produce 2 10^6 cells, i.e. 62 minutes per generation. If ASV 1 (*Aeromonas* sp.) was just below the detection limit ((1/3748*9.78 10^7)/10= 2600), corresponding to an average growth rate of 125 minutes per generation.

STEP4: Assuming that each cell contains 30 fg of carbon, we convert the number of cells produced during the course of the experiment to a total carbon reservoir at the end of the experiment (^{13}C + ^{12}C). *Aeromonas* has 2.09 10^7 cells at the end, and a negligible amount at the beginning (undetectable). We then estimate the amount of total carbon that was captured by the growth of ASV1 (*Aeromonas* sp.). For example, 2.09 10^7 *Aeromonas* cells translate into 6.28 10^{-8} g of total carbon content. It should be noted that 30 fg of carbon was measured for dried *Aeromonas* cells using a Leco CHN analyzer [3] but we assume the same value for every ASV. In the aforementioned work, the cellular carbon content varied between 20 and 40 fg, depending on the bacterial species.

STEP5: using the shifts in buoyant density between the ^{12}C- and the ^{13}C- bottles, we estimate the labeling level of each ASV so that we can estimate their contribution to the ^{13}C mass balance. We compare the buoyant density of each ASV in the ^{13}C bottle to the density of in the ^{12}C bottle by fitting a normal curve to the absolute numbers of 16S rRNA genes that were detected in each fraction. Since we measured the density of each fraction by refractometry, the mean of the normal curve is the best estimate of the actual buoyant density of the ASV (Figure S 3). For example, the 16S DNA of ASV1 (*Aeromonas* sp.) have a mean density of 1.72 in the ^{12}C bottle and 1.75 in the ^{13}C bottle with good fits (R^2=0.98 and 0.89). As mentioned in the text, *ASV2 (Tolumonas* sp.) is not abundant enough in the ^{12}C bottle to fit a normal curve on its distribution across the gradient, so we used its theoretical density based on its GC content (which shows a 15% error). The shift between the ^{12}C- and ^{13}C- densities was converted into a percentage of ^{13}C by dividing by 0.036 [4]. The labeling level of ASV1 (*Aeromonas* sp.) was (1.75-1.72)/0.036=85%.

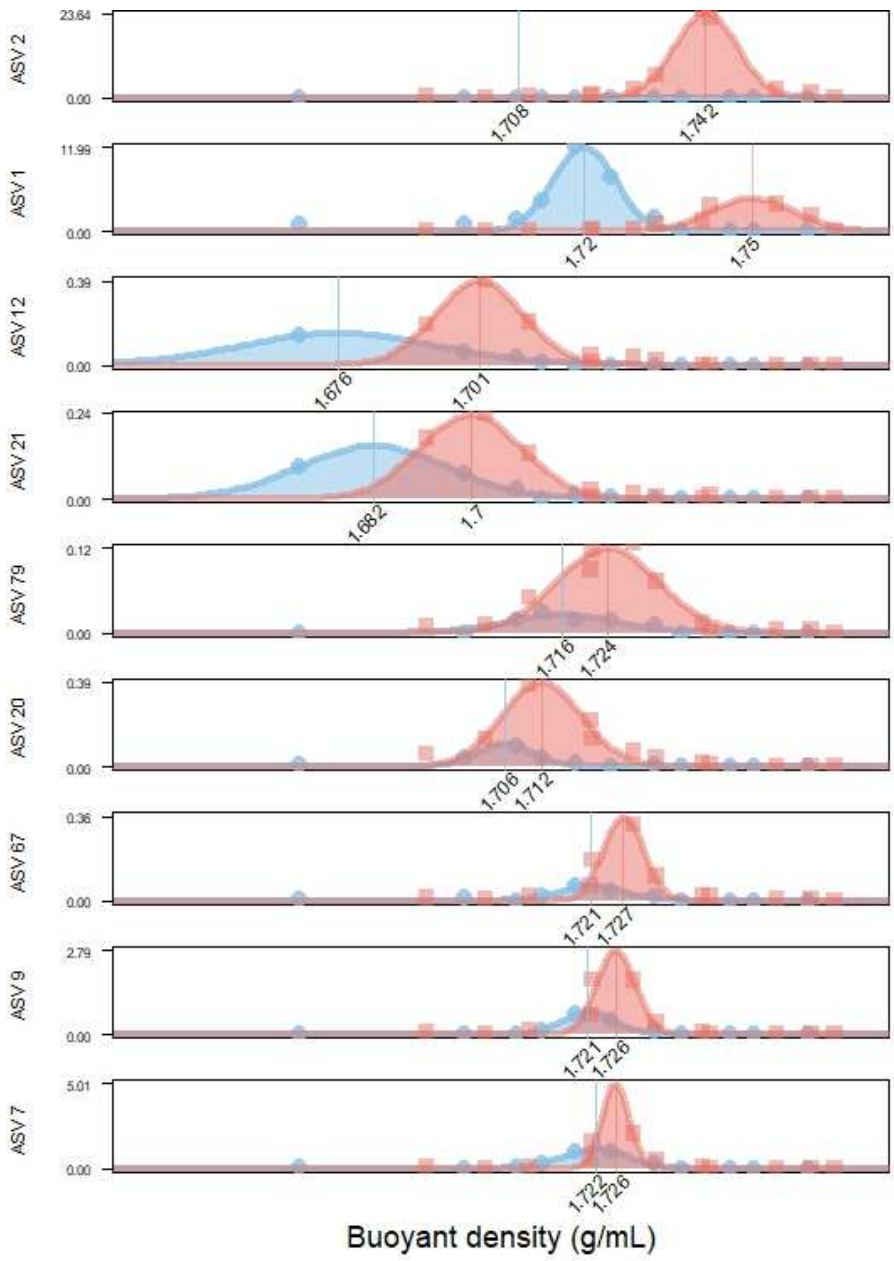

Figure S 3 : Gaussian fits of the 9 most labeled ASVs.

The amount of DNA for the top 9 ASVs (in ng) is plotted against the density of the Cesium gradient (in g/mL). The blue color is in the control bottle. The red color indicates the amount of DNA in the bottle supplemented with 3.2 µg of 13C in the 13C- labeled T4 bacteriophages. The dots indicate the actual measures performed after 24h, i.e. the amount of DNA of each ASV (Qbit was combined with the 16S rDNA sequencing) in each fraction whose density was measured by refractometry. The lines indicate the Gaussian distributions to accurately estimate the mean buoyant density. The mean buoyant density of ASV 2 (Tolumonas sp.) was estimated with the theoretical value in the 12C bottle, as ASV2 did not grow sufficiently in that bottle to fit a reliable Gaussian fit. The pie charts indicate the ratios of the nine 13C-labeled ASV in the 13C and 12C bottles after 24h and their proportion in the initial sample is reported in the X axis. For example, the pie of Aeromonas is roughly balanced because ASV 1 (Aeromonas sp.) represented 19% and 8% in the 12C and 13C bottles respectively. In contrast, ASV 2 (Tolumonas sp.) only grew substantially in the 13C bottle (red).

STEP6: To complete the mass balance of the ^{13}C-atoms of the labeled T4 phages, we multiply the total carbon content of each species by its labeling level. For example, ASV1 (*Aeromonas* sp.) represents $6.28\ 10^{-8}$ x 0.85 = $5.33\ 10^{-8}$ g of carbon (Table S3).

STEP7: To estimate the mass of carbon needed to account for the carbon content observed each species, we assume that the carbon use efficiency for each ASV is 33% (see pure culture experiment). It should be noted that we measured the yield for ASV1 (*Aeromonas* sp.) and we then we assume the same yield for every ASV. Once corrected by the carbon use efficiency (i.e. the bacterial yield), the estimation of ^{13}C needed by each species is compared to the $3.2\ 10^{-6}$ g of ^{13}C incorporated in the $2.28\ 10^{10}$ ^{13}C-labeled T4 phages (since each T4 viral particle contains $1.49\ 10^{-16}$ g C and we assume that they were 100% labeled with ^{13}C because of their production method). For example, we estimated $2.09\ 10^{6}$ newly synthesized cells of ASV1 (*Aeromonas* sp.), which account for $6.28\ 10^{-8}$ g ^{13}C therefore correspond to 5% of the ^{13}C atoms initially present. Adding the contributions of the 9 most-labeled ASVs accounts for 41% of the initial mass of ^{13}C (Table below).

Table S 3 : ^{13}C mass balance of the isotopically labeled T4 bacteriophages.
This table indicates the rationale for the ^{13}C mass balance following the steps described above. For example, ASV 1 (Aeromonas sp.) represents 8% of the 2.47 10^8 16S rDNA copies found at the end of the experiment, which represents 5% of the total amount of ^{13}C present in the initial T4 phages because the 30fgC-cells labeled at 85% needed 5.3 10^{-8}g of ^{13}C if we consider a 33% yield.

STEP	Description	ASV 1	ASV 2	ASV 7	ASV 9	ASV 12	ASV 20	ASV 21	ASV 67	ASV 79
1	Absolute number of 16S rDNA copies in the initial sample	9.78 10^7								
	Absolute number of 16S rDNA copies in the final sample	2.47 10^8								
2	Counts in the initial sample (out of 3748 sequences)	0	0	148	132	197	123	0	46	53
	Counts in the final ^{13}C sample (out of 3578 sequences)	303	1545	37	62	52	55	55	41	55
	Relative initial abundance of 16S rDNA of each ASV	0%	0%	4%	4%	5%	3%	0%	1%	1%
	Relative final abundance of 16S rDNA of each ASV	8%	43%	1%	2%	1%	2%	2%	1%	2%
	Absolute number of 16S rDNA copies in the initial sample of each ASV	0	0	3.86 10^6	3.44 10^6	5.14 10^6	3.21 10^6	0	1.20 10^6	1.38 10^6
	Absolute number of 16S rDNA copies in the final sample of each ASV	2.09 10^7	1.07 10^8	2.55 10^6	4.28 10^6	3.59 10^6	3.80 10^6	3.80 10^6	2.83 10^6	3.80 10^6
	Number of newly synthetized 16S copies	2.09 10^7	1.07 10^8	0	8.36 10^5	0	5.87 10^5	3.80 10^6	1.63 10^6	2.41 10^6
3	Number of 16S rDNA copies per genome of each ASV [2]	10	10	4	4	1	2	1	2	2
	Number of newly synthetized cells of each ASV	2.09 10^6	1.07 10^7	0	2.09 10^5	0	2.94 10^5	3.80 10^6	8.15 10^5	1.21 10^6
4	Carbon content (g/cell)	3.00 10^{-14}								
	Total Carbon content in each ASV (g)	6.28 10^{-8}	3.20 10^{-7}	0	6.27 10^{-9}	0	8.81 10^{-9}	1.14 10^{-7}	2.45 10^{-8}	3.62 10^{-8}
5	Mean 12C density (g/mL)	1.72	1.7	1.72	1.72	1.68	1.71	1.68	1.72	1.72
	Goodness_fit_in_^{12}C (R^2)	0.98	0.4	0.99	0.97	0.99	0.97	0.98	0.88	0.89
	Mean corrected ^{12}C density	1.72	1.71	1.72	1.72	1.68	1.71	1.68	1.72	1.72
	Mean ^{13}C density	1.75	1.74	1.73	1.73	1.7	1.71	1.7	1.73	1.72
	Goodness_fit_in_^{13}C (R^2)	0.89	0.99	0.9	0.89	0.98	0.93	0.99	0.94	0.94
	Labeling Level (%)	85%	95%	10%	14%	71%	19%	49%	16%	23%
6	^{13}C carbon content in each ASV (g)	5.3 10^{-8}	3.0 10^{-7}	0	8.8 10^{-10}	0	1.7 10^{-9}	5.6 10^{-8}	3.9 10^{-9}	8.3 10^{-9}
7	Carbon use efficiencicy (i.e. Bacterial yield)	0.33								
	Contribution to the ^{13}C mass balance (out of the 3.2 µg of ^{13}C in the bacteriophages)	5%[1]	29%[1]	0%[1]	0%[1]	0%	0%	5%	0%	1%
	^{13}C mass balance	41%								

[1], 83% of the predation of T4 phages is due to *Gammaproteobacteria*, which also include *E. coli*, the natural host of T4 phages.

1.3 Taxonomy of the ^{13}C-labeled ASVs

Table S 4 : Taxonomic affiliation of the ASVs that are significantly labeled with ^{13}C

This table indicates the taxonomy of the labeled ASV performed by DADA2 with the Siva138 dataset. The taxonomy was also checked by blasting on the NCBI database.

seq_ID.x	Class	Order	Family	Genus
ASV 2	Gammaproteobacteria	Aeromonadales	Aeromonadaceae	Tolumonas
ASV 1	Gammaproteobacteria	Aeromonadales	Aeromonadaceae	Aeromonas
ASV 12	Ignavibacteria	Ignavibacteriales	PHOS-HE36	NA
ASV 21	Ignavibacteria	Ignavibacteriales	PHOS-HE36	NA
ASV 79	Bacteroidia	Chitinophagales	Saprospiraceae	Haliscomenobacter
ASV 20	Bacteroidia	Chitinophagales	Saprospiraceae	NA
ASV 67	Anaerolineae	Ardenticatenales	NA	NA
ASV 7	Gammaproteobacteria	Burkholderiales	Rhodocyclaceae	NA
ASV 9	Gammaproteobacteria	Burkholderiales	Rhodocyclaceae	Dechloromonas

2 Isolation of Aeromonas_isolate_007 and subsequent experiments

Following the SIP experiment, we could luckily isolate a strain of Aeromonas sp (ASV1) from the initial sample using the Aeromonas Isolation Agar medium (Sigma 17118) with ampicillin since Aeromonads are resistant to ampicillin. Therefore, we could confirm that *Aeromonas* sp. was indeed able to assimilate the carbon of the T4 phages. Furthermore, we could show that *Aeromonas* could use T4 phages as carbon and nitrogen source with a 33% yield and scan the genome of Aeromonas_isolate_007 for putative mechanisms by which *Aeromonas* could capture, digest the T4 phage proteins and transfer the generated peptides into the intracellular space.

2.1 Pure culture experiment

We incubated 50 *Aeromonas* cells with 10^{11} T4 phages in 1mL. After 24h, we counted 1.63 10^{8} Aeromonas cells. Converting 10^{11} T4 phages into 1.6 10^{8} ASV1 (*Aeromonas* sp.) cells (Figure S 4) corresponds to 9.14 10^{-14} g of carbon (613 bacteriophages of 1.49 10^{-16} gC) per *Aeromonas* cell containing 3 10^{-14} of carbon, hence a carbon use efficiency of 33% (also called bacterial yield). The number of generations in 2880 minutes was estimated to (ln 1.6 10^{8}/58)/ln(2) = 21.3, hence 134 minutes per generation.

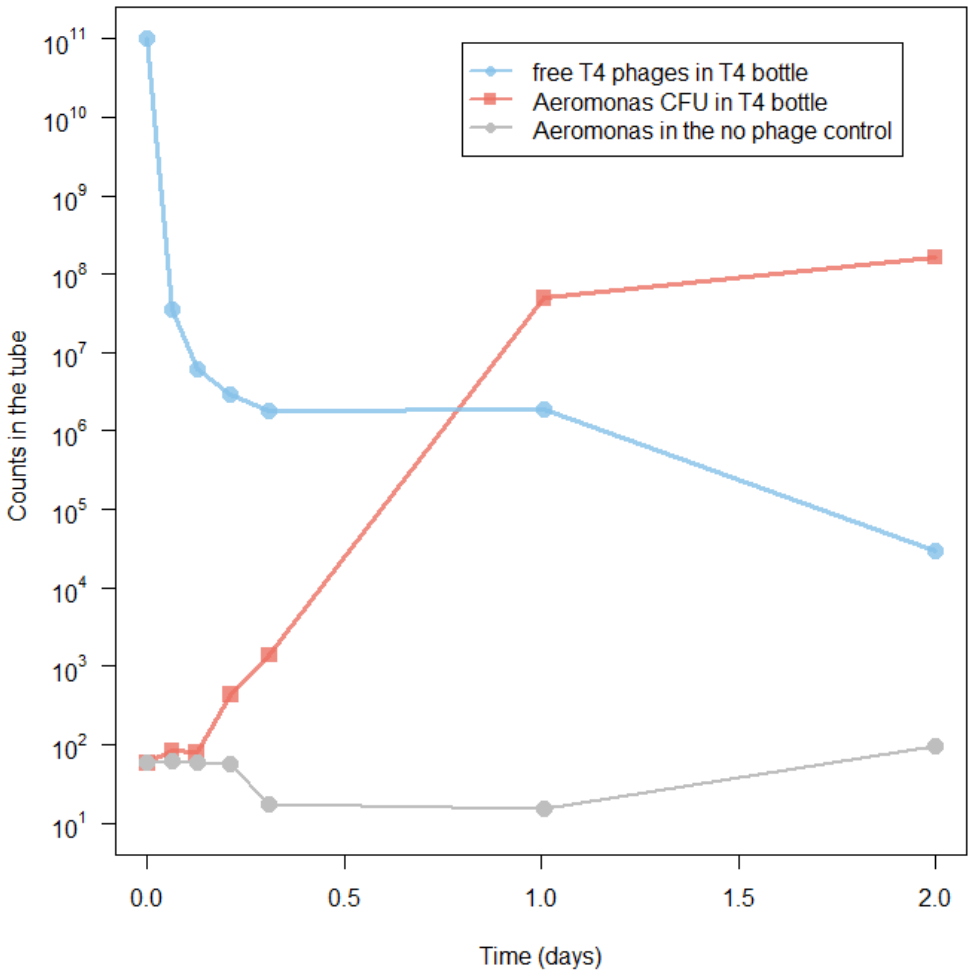

Figure S 4 : Bacteriophage decrease and Aeromonas_isolate_007 growth in pure culture

The red line indicates the number of colony-forming units over time when 50 Aeromonas cells are supplemented with 10^{11} T4 bacteriophages (blue line). The grey line demonstrates that the SM buffer in which the T4 bacteriophages are conserved is not responsible for the growth.

2.2 Whole genome sequencing

2.2.1 Sequencing technique and statistics

The whole genome sequencing was performed on the GeT-Plage facility in Toulouse.

Briefly, Aeromonas DNA was fragmented by sonication and sequencing adaptators were ligated. 8 cycles of PCR were applied to amplify libraries. Library quality was assessed using an Advanced Analytical Fragment Analyzer and libraries were quantified by QPCR using the Kapa Library Quantification Kit. DNA-seq experiments were performed on an Illumina Miseq using a paired-end read length of 2x300 pb with the Illumina MiSeq Reagent Kits v3. The sequences were quality trimmed with fastp v0.20.0[5], assembled by Spades v3.14.1[6] after removing the residual phiX by using bowtie2 v2.3.5.1[7], and filtering scaffolds smaller than right insert size quantile 525nt and coverage smaller than 50X. The assembly statistics of the *Aeromonas* genome are below:

- Total genome size : 4667413 nt
- Max scaffold size : 1964260 nt
- Min scaffold size (after scaffold coverage and size filtering) : 504 nt
- Nb scaffold : 29
- Nb contig : 31
- N50 scaffold size : 947468 nt
- Average scaffold size : 160945.28 nt
- Nb Total gene : 4172
- % complete gene : 99.73
- 16S rRNA nb fragment : 2
- 16S rRNA fragment size : 1016 nt + 531 nt
- nb of 16S rRNA copies based on ratio with scaffold coverage : 10.89
- nb of 16S rRNA copies based on reference database [2]: 10

2.2.2 Phylogenetic tree of Aeromonas_isolate_007

The whole genome sequencing of the Aeromonas_isolate_007 by Illumina Miseq narrows down the phylogeny of the strain and offers suggestions with respect to degradative enzymes that may help bacteriophage digestion Table S5).

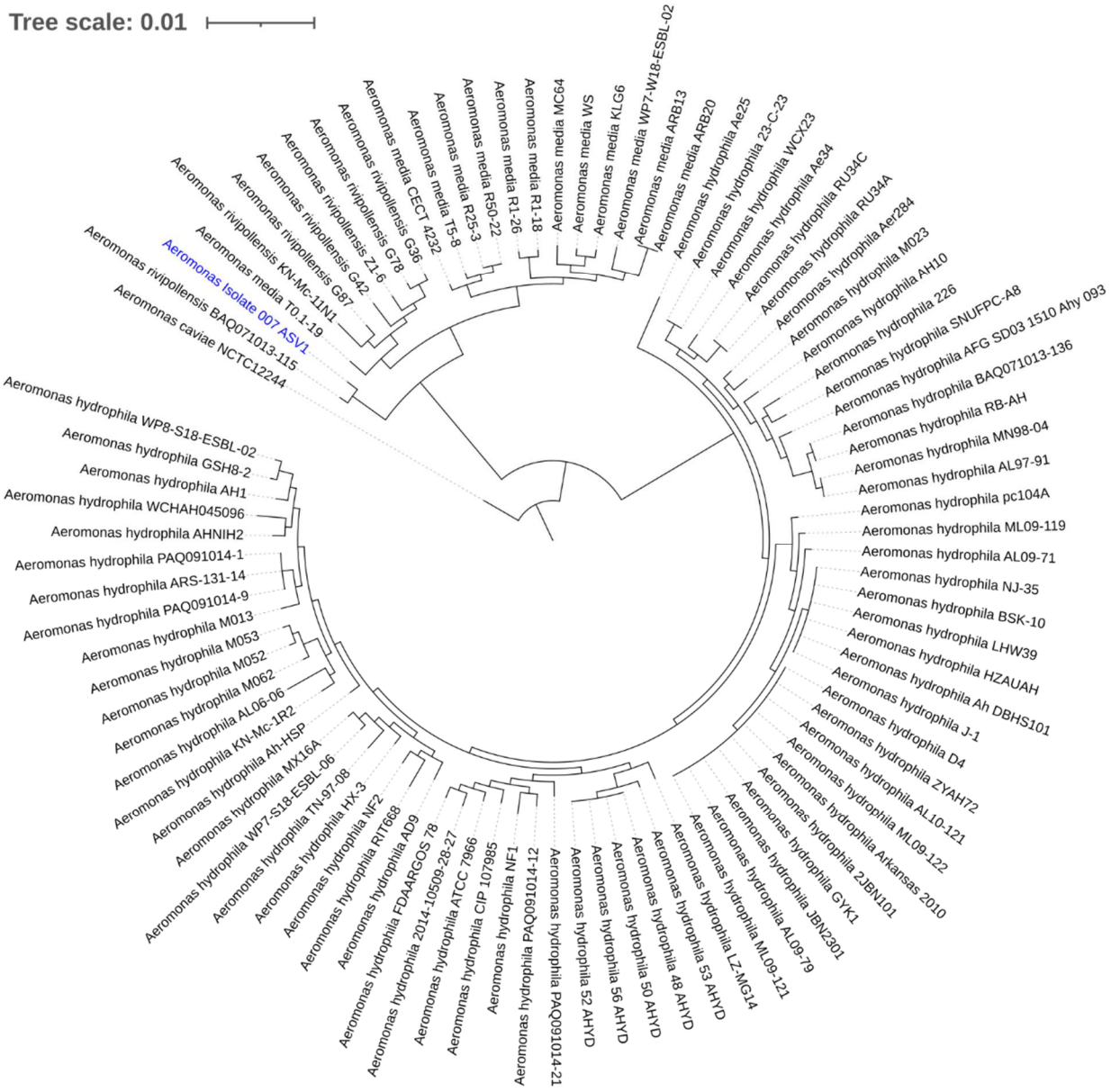

Figure S 5 : Phylogenetic tree of Aeromonas_Isolate_007_151020

The analysis of the whole genome confirms that Aeromonas_Isolate_007_151020 belongs to an intermediate clade between Aeromonas media and Aeromonas rivipollensis species.

2.2.3 Schematic model of the phage predation

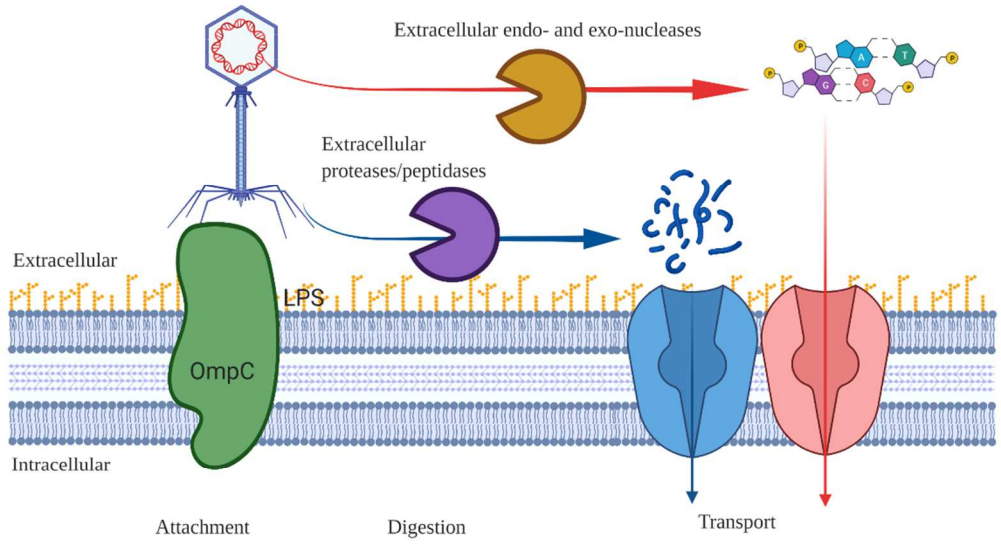

Figure S6: Schematic representation of the capture, digestion and absorption of the T4 phages by Aeromonas sp

Since T4 phages are large particles (not to scale in the figure)., we assume that Aeromonas captures the T4 phages due to its similarity with the cell wall of E.coli. Once captured, the proteins of the capsid may be digested by the extracellular proteases present in Aeromonas sp and the DNA could be degraded as well. The products of these degradations could be ingested by Aeromonas via common transporters.

2.2.4 Annotation of the putative genes involved in phage predation

The functional annotation was performed with RAST8, eggNOG-mapper (v2.0.0)9 and TMHMM10 to predict the extracellular location of the proteins. The results are reported in the table below.

Table S 5 : Annotation of the Aeromonas proteins putatively involved in the capture, digestion and absorption of T4 phages, which are reported in the table below.

Putative function	RAST protein id	contig id	RAST_function	TMHMM inside	TMHMM transmembrane	TMHMM outside
CAPTURE	fig|642.770.peg.2774	NODE_2_length_94746 8_cov_91.192050	Outer_membrane_porin_OmpC	1	1	1
	fig|642.770.peg.1967	NODE_1_length_1964260_cov_90.024368		0	0	1
	fig|642.770.peg.3181	NODE_3_length_439005_cov_94.027299		0	0	1
Extracellular DIGESTION of large proteins	fig|642.770.peg.202	NODE_1_length_1964260_cov_90.024368	putative_extracellular_serine_protease	0	0	1
	fig|642.770.peg.309	NODE_1_length_1964260_cov_90.024368	Uncharacterized_protease_YhbU	0	0	1
	fig|642.770.peg.653	NODE_1_length_1964260_cov_90.024368	Tail-specific_protease_precursor_(EC_3.4.21.102)	0	0	1
	fig|642.770.peg.664	NODE_1_length_1964260_cov_90.024368	Lon_protease_homolog_YcbZ	0	0	1
	fig|642.770.peg.903	NODE_1_length_1964260_cov_90.024368	ATP-dependent_protease_La_(EC_3.4.21.53)_Type_I	0	0	1
	fig|642.770.peg.904	NODE_1_length_1964260_cov_90.024368	ATP-dependent_Clp_protease_ATP-binding_subunit_ClpX	0	0	1
	fig|642.770.peg.905	NODE_1_length_1964260_cov_90.024368	ATP-dependent_Clp_protease_proteolytic_subunit_ClpP_(EC_3.4.21.92)	0	0	1
	fig|642.770.peg.919	NODE_1_length_1964260_cov_90.024368	Protease_III_precursor_(EC_3.4.24.55)	0	0	1
	fig|642.770.peg.976	NODE_1_length_1964260_cov_90.024368	ATP-dependent_Clp_protease_ATP-binding_subunit_ClpA	0	0	1
	fig|642.770.peg.1312	NODE_1_length_1964260_cov_90.024368	Protease_II_(EC_3.4.21.83)	0	0	1
	fig|642.770.peg.1793	NODE_1_length_1964260_cov_90.024368	Uncharacterized_protease_YegQ	0	0	1
	fig|642.770.peg.1989	NODE_1_length_1964260_cov_90.024368	Vibriolysin__extracellular_zinc_protease_(EC_3.4.24.25)_@_Pseudolysin__extracellular_zinc_protease_(EC_3.4.24.26)	0	0	1
	fig|642.770.peg.2147	NODE_2_length_94746 8_cov_91.192050	Uncharacterized_protease_YdcP	0	0	1
	fig|642.770.peg.3280	NODE_3_length_439005_cov_94.027299	Protease_II_(EC_3.4.21.83)	0	0	1
	fig|642.770.peg.3795	NODE_5_length_206066_cov_93.597574	ATP-dependent_hsl_protease_ATP-binding_subunit_HslU	0	0	1
	fig|642.770.peg.3796	NODE_5_length_206066_cov_93.597574	ATP-dependent_protease_subunit_HslV_(EC_3.4.25.2)	0	0	1
	fig|642.770.peg.12	NODE_10_length_72653_cov_95.226534	Oligopeptidase_A_(EC_3.4.24.70)	0	0	1
	fig|642.770.peg.67	NODE_10_length_72653_cov_95.226534	Xaa-Pro_dipeptidase_PepQ_(EC_3.4.13.9)	0	0	1
	fig|642.770.peg.308	NODE_1_length_1964260_cov_90.024368	Uncharacterized_peptidase_U32_family_member_YhbV	0	0	1
	fig|642.770.peg.319	NODE_1_length_1964260_cov_90.024368	Peptidase_B_(EC_3.4.11.23)	0	0	1
	fig|642.770.peg.324	NODE_1_length_1964260_cov_90.024368	Peptidase_B_(EC_3.4.11.23)	0	0	1

	fig|642.770.peg.496	NODE_1_length_1964260_cov_90.024368	Aminopeptidase_PepA-related_protein	0	0	1
	fig|642.770.peg.654	NODE_1_length_1964260_cov_90.024368	Membrane_alanine_aminopeptidase_N_(EC_3.4.11.2)	0	0	1
	fig|642.770.peg.1189	NODE_1_length_1964260_cov_90.024368	Oligoendopeptidase_F-like_protein	0	0	1
	fig|642.770.peg.1360	NODE_1_length_1964260_cov_90.024368	Tripeptide_aminopeptidase_(EC_3.4.11.4)	0	0	1
	fig|642.770.peg.1462	NODE_1_length_1964260_cov_90.024368	Probable_endopeptidase_NlpC	0	0	1
Extracellular DIGESTION of large proteins	fig|642.770.peg.1502	NODE_1_length_1964260_cov_90.024368	FIG009095:_D_D-carboxypeptidase_family_protein	0	0	1
	fig|642.770.peg.1638	NODE_1_length_1964260_cov_90.024368	Peptidase__M23/M37_family	0	0	1
	fig|642.770.peg.1722	NODE_1_length_1964260_cov_90.024368	Membrane_proteins_related_to_metalloendopeptidases	0	0	1
	fig|642.770.peg.1792	NODE_1_length_1964260_cov_90.024368	L_D-transpeptidase_>_YbiS	0	0	1
	fig|642.770.peg.1981	NODE_1_length_1964260_cov_90.024368	L_D-transpeptidase_>_YbiS	0	0	1
	fig|642.770.peg.2129	NODE_2_length_947468_cov_91.192050	Alpha-aspartyl_dipeptidase_Peptidase_E_(EC_3.4.13.21)	0	0	1
	fig|642.770.peg.2153	NODE_2_length_947468_cov_91.192050	Thermostable_carboxypeptidase_1_(EC_3.4.17.19)	0	0	1
	fig|642.770.peg.2266	NODE_2_length_947468_cov_91.192050	Methionine_aminopeptidase_(EC_3.4.11.18)	0	0	1
	fig|642.770.peg.2291	NODE_2_length_947468_cov_91.192050	Peptidase__M13_family	0	0	1
	fig|642.770.peg.2456	NODE_2_length_947468_cov_91.192050	γ-glutamyltranspeptidase_(EC_2.3.2.2)_@_Glutathione_hydrolase_(EC_3.4.19.13)	0	0	1
	fig|642.770.peg.3506	NODE_4_length_411610_cov_92.800192	Xaa-Pro_aminopeptidase_(EC_3.4.11.9)	0	0	1
	fig|642.770.peg.3576	NODE_4_length_411610_cov_92.800192	Prolyl_endopeptidase_(EC_3.4.21.26)	0	0	1
	fig|642.770.peg.4017	NODE_6_length_154685_cov_89.330397	Oligoendopeptidase_F-like_protein	0	0	1
	fig|642.770.peg.4147	NODE_7_length_126480_cov_93.962673	Bacterial_leucyl_aminopeptidase_(EC_3.4.11.10)	0	0	1
DNA DIGESTION	fig|642.770.peg.760	NODE_1_length_1964260_cov_90.024368	Extracellular_and/or_outer_membrane_deoxyribonuclease_NucH/SO1066	0	0	1
	fig|642.770.peg.1409	NODE_1_length_1964260_cov_90.024368	UPF0294_protein_YafD (exo- and endo- nuclease family)	0	0	1
	fig|642.770.peg.1884	NODE_1_length_1964260_cov_90.024368	DNA/RNA_endonuclease_G	1	1	1
	fig|642.770.peg.1925	NODE_1_length_1964260_cov_90.024368	Extracellular_and/or_outer_membrane_deoxyribonuclease_NucH/SO1066	0	0	1
Peptide TRANSPORT into the cell	fig|642.770.peg.2135	NODE_2_length_947468_cov_91.192050	Succinyl-CoA_synthetase__alpha_subunit	0	0	1
	fig|642.770.peg.274	NODE_1_length_1964260_cov_90.024368	ABC_transporter__permease_protein_1_(cluster_5__nickel/peptides/opines)	4	6	3
	fig|642.770.peg.275	NODE_1_length_1964260_cov_90.024368	ABC_transporter__permease_protein_2_(cluster_5__nickel/peptides/opines)	3	5	3
	fig|642.770.peg.1213	NODE_1_length_1964260_cov_90.024368	Oligopeptide_ABC_transporter__permease_protein_OppC_(TC_3.A.1.5.1)	4	6	3
	fig|642.770.peg.1214	NODE_1_length_1964260_cov_90.024368	Oligopeptide_ABC_transporter__permease_protein_OppB_(TC_3.A.1.5.1)	4	6	3
	fig|642.770.peg.1215	NODE_1_length_1964260_cov_90.024368	Oligopeptide_ABC_transporter__substrate-binding_protein_OppA_(TC_3.A.1.5.1)	1	1	1
	fig|642.770.peg.1819	NODE_1_length_1964260_cov_90.024368	Dipeptide_ABC_transporter__permease_protein_DppC_(TC_3.A.1.5.2)	4	6	3
	fig|642.770.peg.1820	NODE_1_length_1964260_cov_90.024368	ABC_transporter__permease_protein_1_(cluster_5__nickel/peptides/opines)	4	6	3
	fig|642.770.peg.1913	NODE_1_length_1964260_cov_90.024368	ABC_transporter__permease_protein_2_(cluster_5__nickel/peptides/opines)	4	6	3
	fig|642.770.peg.1914	NODE_1_length_1964260_cov_90.024368	ABC_transporter__permease_protein_1_(cluster_5__nickel/peptides/opines)	4	6	3

DNA TRANSPORT into the cell	fig|642.770.peg.2922	NODE_3_length_439005_cov_94.027299	Na+_dependent_nucleoside_transporter_NupC	5	9	4
	fig|642.770.peg.2967	NODE_3_length_439005_cov_94.027299	Na+_dependent_nucleoside_transporter_NupC	4	8	4
	fig|642.770.peg.3112	NODE_3_length_439005_cov_94.027299	Na+_dependent_nucleoside_transporter_NupC	4	8	4
	fig|642.770.peg.4145	NODE_7_length_126480_cov_93.962673	Predicted_nucleoside_ABC_transporter__permease_1_component	6	10	5
	fig|642.770.peg.4146	NODE_7_length_126480_cov_93.962673	Predicted_nucleoside_ABC_transporter__permease_2_component	4	7	4
	fig|642.770.peg.177	NODE_13_length_22868_cov_91.969299	DNA_uptake_protein	0	0	1

3 REFERENCES

1 Zemb, O. *et al.* Absolute quantitation of microbes using 16S rRNA gene metabarcoding: A rapid normalization of relative abundances by quantitative PCR targeting a 16S rRNA gene spike-in standard. *Microbiologyopen* **9**, doi:10.1002/mbo3.977 (2020).

2 Větrovský, T. & Baldrian, P. The Variability of the 16S rRNA Gene in Bacterial Genomes and Its Consequences for Bacterial Community Analyses. *PLOS ONE* **8**, e57923, doi:10.1371/journal.pone.0057923 (2013).

3 Trousselier, M., Bouvy, M., Courties, C. & Dupuy, C. Variation of carbon content among bacterial species under starvation condition. *Aquatic Microbial Ecology* (1997).

4 Buckley, D. H., Huangyutitham, V., Hsu, S. F. & Nelson, T. A. Stable isotope probing with 15N achieved by disentangling the effects of genome G+C content and isotope enrichment on DNA density. *Appl Environ Microbiol* **73**, 3189-3195, doi:10.1128/aem.02609-06 (2007).

5 Chen, S., Zhou, Y., Chen, Y. & Gu, J. fastp: an ultra-fast all-in-one FASTQ preprocessor. *Bioinformatics* **34**, i884-i890, doi:10.1093/bioinformatics/bty560 (2018).

6 Prjibelski, A., Antipov, D., Meleshko, D., Lapidus, A. & Korobeynikov, A. Using SPAdes De Novo Assembler. *Current protocols in bioinformatics* **70**, e102, doi:10.1002/cpbi.102 (2020).

7 Langmead, B. & Salzberg, S. L. Fast gapped-read alignment with Bowtie 2. *Nat Methods* **9**, 357-359, doi:10.1038/nmeth.1923 (2012).

8 Aziz, R. K. *et al.* The RAST Server: rapid annotations using subsystems technology. *BMC Genomics* **9**, 75, doi:10.1186/1471-2164-9-75 (2008).

9 Muller, J. *et al.* eggNOG v2.0: extending the evolutionary genealogy of genes with enhanced non-supervised orthologous groups, species and functional annotations. *Nucleic Acids Res* **38**, D190-195, doi:10.1093/nar/gkp951 (2010).

10 Krogh, A., Larsson, B., von Heijne, G. & Sonnhammer, E. L. Predicting transmembrane protein topology with a hidden Markov model: application to complete genomes. *J Mol Biol* **305**, 567-580, doi:10.1006/jmbi.2000.4315 (2001).